Pore Size Distribution Analysis of Microporous Carbons: A Density Functional Theory Approach

Christian Lastoskie,[†] Keith E. Gubbins,[*,†] and Nicholas Quirke[†,‡]

School of Chemical Engineering, Cornell University, Ithaca, New York 14853, and BP Research Centre, Middlesex TW16 7LN, U.K.

Received: December 4, 1992

We present an improved method, based upon density functional theory, for the determination of the pore size distribution (PSD) of porous sorbents. The adsorption isotherms predicted by nonlocal mean field theory for individual slit pores are correlated as a function of pressure and pore width. The PSD is then calculated by fitting this correlation to the experimental adsorption isotherm of the sorbent. We apply the analysis method to adsorption data for nitrogen on several porous carbons. In this application, the porous network is modeled as a continuous size distribution of noninteracting slit-shaped graphitic pores. The PSDs obtained by using the Kelvin equation and using the local and nonlocal versions of the mean field density functional theory are compared and evaluated. The results demonstrate that nonlocal theory provides a more accurate interpretation of the PSD than previous methods have achieved, particularly when the analysis is applied to highly microporous sorbents.

1. Introduction

Industrial sorbents such as activated carbons, silica gels, activated aluminas, zeolites, and molecular sieve carbons are employed in a multitude of gas separation, purification, and reaction processes. The adsorption and transport behavior of fluids in these porous sorbents depend largely upon the number and size of the various pores present in the material. Hence, in order to develop a useful predictive model of sorbent adsorptive and catalytic properties, it is important to establish the pore size distribution (PSD) of the sorbent. By IUPAC convention,[1] the range of pore sizes is divided into the groups shown in Table I.

Nitrogen adsorption measurements are routinely used for determining the PSD of mesoporous carbons. The experimental nitrogen isotherm is a composite of the individual adsorption isotherms of the various sizes of pores present in the sorbent. Hence, in order to calculate the distribution of pore sizes, it is necessary to develop a model for pore filling which relates the pore width to the condensation pressure. Historically, the Kelvin equation has been the most commonly employed model. For completely wet slit-shaped pores, the Kelvin equation is

$$\ln(P_C/P_0) = -2\gamma_l/RT\rho_l H \qquad (1)$$

where P_C is the pressure at which a pore of width H condenses, P_0 is the saturation pressure of the bulk fluid, R is the ideal gas constant, and ρ_l and γ_l are the liquid density and surface tension of nitrogen at absolute temperature T. The Kelvin equation is derived from classical thermodynamics and assumes that surface tension can be defined and that the gas phase is ideal; it is accurate in the limit of large pores where P_C approaches P_0. It fails, however, when applied to narrow pores; in particular, the equation does not take into account the thickness of the layers formed on the porous surface prior to condensation. A variety of methods[2,3] attempt to account for film growth by coupling the Kelvin equation with a standard isotherm, or "t-curve", to describe the thickness of the precondensation film on the pore walls. The standard isotherm is measured on a nonporous carbon surface; thus, film growth on the walls of a slit pore can be modeled by the standard isotherm only if the slit is sufficiently wide so that adsorbed films on opposing walls do not interact with each other. For micropores, which have widths on the order of just a few molecular diameters, this assumption is incorrect. Adsorption is enhanced in narrow pores due to increased interactions between adsorbed films on opposing walls and also because of stronger solid-fluid attractive forces resulting from the overlap of the wall potentials. Therefore, adsorption models based upon the Kelvin equation and the standard isotherm overestimate the pressures at which film wetting and capillary condensation occur. Consequently, PSD methods using Kelvin-type adsorption models underestimate the sizes of the pores present in the sorbent. Simulation studies[4] suggest that 75 Å is the approximate lower bound on the range of pore sizes that can be reliably determined from classical thermodynamic analysis methods.

TABLE I: IUPAC Classification of Pore Sizes

type	pore size (Å)
macropore	≥ 500
mesopore	20 to 500
supermicropore	7 to 20
ultramicropore	≤ 7

A corrected Kelvin equation may be obtained by modifying the effective pore width used in the Kelvin equation calculation of the filling pressure by allowing for the film thickness already adsorbed before condensation occurs. The "modified" Kelvin equation has the form

$$\ln(P_C/P_0) = -2\gamma_l/RT\rho_l(H - nt) \qquad (2)$$

where t is the equilibrium film thickness at condensation pressure P_C and n assumes a value of 2 or 3 depending on the choice of method.[5] Introducing this correction lowers the filling pressures and thus somewhat improves the adsorption model for PSD fitting. Nonetheless, the modified Kelvin equation suffers the same defects as the original Kelvin equation when applied to narrow pore sizes, where film interactions are significant. Indeed, for fluids in pore widths of a few molecular diameters, the "texture" of the fluid becomes so pronounced that the concept of a smooth liquid–vapor interface cannot realistically be applied.

Alternative methods have been proposed to determine the PSD of microporous sorbents from adsorption experiments. One semiempirical approach is to combine the Dubinin–Astakhov equation for estimating micropore volume with an assumed Gaussian micropore size distribution, yielding the so-called Dubinin–Stoeckli equation.[6] This method has two principal

[†] Cornell University.
[‡] BP Research Centre.

0022-3654/93/2097-4786$04.00/0

drawbacks: it constrains the PSD to an arbitrarily chosen functional form, and it requires the use of empirical energy parameters in the solution of the PSD.

A related method, originating from the microporosity model put forth by Everett and Powl,[7] is to calculate an average potential function inside the micropore. By use of thermodynamic arguments, this average potential can be related to the free energy change of adsorption, yielding a relation between filling pressure and pore width. This approach was developed for modeling slitlike pores,[8] and later extended to cylindrical pores.[9] Because this method allows for the importance of the solid–fluid attractive forces in narrow pores, it provides a better measure of the micropore filling pressures. However, the "potential" model gives poor results for larger pores and must be combined with a Kelvin-type method[10] to describe the full range of pore sizes. Furthermore, several of the physical parameters of the interaction potential are difficult to estimate.

Although the measurement of nitrogen isotherms is the most generally applicable method for determining PSDs, several other experimental methods are available for particular kinds of materials or for specific ranges of pore size. Thus helium adsorption[11] has been used to measure ultramicropores, and mercury porosimetry[12] and NMR spin-lattice relaxation[13] provide a means to measure macropores. X-ray diffraction (XRD) has been widely used to determine pore sizes in well-ordered materials, such as zeolites and aluminophosphates,[14] and both XRD and small angle neutron scattering have been used for partially ordered porous materials, such as pillared clays,[15] silica gels,[16] and sol–gel systems.[17] Calorimetric data provide a further source of potential information on the PSD. All of these experimental probes require models of the microstructure in order to interpret the data and obtain information on pore sizes.

In this work we present a PSD analysis method based on nonlocal density functional theory for the interpretation of nitrogen adsorption isotherms based on a slit pore model of the microstructure. The remainder of our paper is organized as follows. In the next section, we develop a model for single pore adsorption using density functional theory. In section 3, we compare and discuss model isotherms generated from density functional theory and classical thermodynamics methods. In section 4, we apply the model isotherms to evaluate the pore size distributions of several porous carbons. The mathematical requirements of solving for the carbon PSDs are also addressed in this section. Finally, in section 5 we summarize our results and offer recommendations for additional improvements in PSD calculation techniques.

2. Molecular Theory of Adsorption

2.1. The Independent Pore Model. In contrast to macroscopic models such as the Kelvin equation or experimental correlations patterned after the Dubinin-type equations, statistical mechanics provides a microscopic model of adsorption. Using Monte Carlo simulation, molecular dynamics, density functional theory, or other methods grounded in statistical mechanics, it is possible to calculate equilibrium sorbent properties such as the adsorption isotherm, heat of adsorption, neutron scattering pattern, and transport properties for model systems. In the approach we adopt here, which we term the *independent pore model*, the general procedure is as follows:

(1) Define the interaction potentials for the fluid–sorbent and fluid–fluid interactions. The fluid interactions with the sorbent will depend, among other things, upon the structure and chemical nature of the surface, the shapes and sizes of the pores in the material, and the connectivity of the porous network.

(2) Apply statistical mechanics to calculate the sorbent property (which we shall denote ψ) for individual pores of size H, shape (denoted symbolically as g), and surface interaction ϕ_{sf} (the solid–fluid intermolecular potential, which in general depends on the surface location), at specified temperature T and pressure P.

(3) Calculate the overall sorbent property ψ_t at state conditions T and P by integrating the individual pore properties over the distribution of pore sizes, pore shapes, and chemical surfaces; symbolically

$$\psi_t(T,P) = \int\int\int \psi(H,g,\phi_{sf};T,P) f(H,g,\phi_{sf})\, dH\, dg\, d\phi_{sf} \quad (3)$$

In practice, the distribution information $f(H,g,\phi_{sf})$ is rarely available from experiment for such calculations. Instead, one can fit the model results for individual pores to experimental property data to extract desired distribution information. For highly ordered crystalline sorbents such as zeolites and aluminophosphates, this procedure can yield detailed structural information. Activated carbons and silicas, by contrast, are less well ordered sorbents that generally possess a broader distribution of pore sizes, geometries, and so on. For these sorbents it is more difficult to characterize the complete distribution function $f(H,g,\phi_{sf})$. In order to render the problem tractable, we propose to replace (3) by the simpler equation

$$\psi_t(T,P) = \int \psi(H;g,\phi_{sf},T,P) f(H)\, dH \quad (4)$$

where $f(H)$ is the PSD. Equation 4 will be correct for materials having a single pore geometry and homogeneous surfaces. For real materials, in which geometric and chemical heterogeneity occurs, we regard $f(H)$ as giving the PSD for an *effective porous material*, in which all of the heterogeneity of the real material is approximated by a distribution of pore sizes.

The mean field density functional theory method proposed by Seaton, Walton, and Quirke[18] is a novel statistical mechanical attempt to extend the accuracy of PSD analysis in both the mesopore and micropore range. In their analysis, Seaton et al. employ local mean field theory (outlined in section 2.3) to model the fluid adsorption within the pore. Local mean field theory provides an accurate description of mesopore filling and some of the qualitative features of micropore adsorption. For example, the local theory predicts enhanced uptake in micropores at low pressures due to potential enhancement and shows the expected thickening of the adsorbed film in mesopores as pressure is increased. Local theory also correctly exhibits a transition from capillary condensation in large pores to continuous filling in small pores. While the local theory model becomes increasingly inaccurate for very small pore sizes because of the importance of short-ranged correlations in these pores (see section 3), the local theory nevertheless represents a substantial improvement over the classical thermodynamic description of pore filling, and it has been used to predict methane uptake in activated carbons.[19]

To solve for the PSDs of porous carbons, Seaton et al. fitted model isotherms to experimental nitrogen uptake measurements. Mathematically, the experimental isotherm $N(P)$ is expressed as (see eq 4)

$$N(P) = \int_{H_{min}}^{H_{max}} \rho(P,H) f(H)\, dH \quad (5)$$

where H_{min} and H_{max} are the widths of the smallest and largest pores considered in the analysis, $\rho(P,H)$ is the mean density of nitrogen in a pore of width H at pressure P, and $f(H)$ is the pore size distribution of the porous carbon. The density functional theory provides the individual pore isotherms $\rho(P,H)$, which are then applied to the experimental adsorption measurements in the numerical solution of the integral to obtain the pore size distribution $f(H)$.

In this work, we extend the analysis method of Seaton et al. by adopting a nonlocal mean field density functional theory model of adsorption. Local mean field theory neglects short-ranged correlations in the fluid density and hence cannot reproduce the strong oscillations characteristic of the fluid density profile at a solid–fluid interface. The nonlocal version of the mean field theory, developed in section 2.3, provides a quantitatively accurate

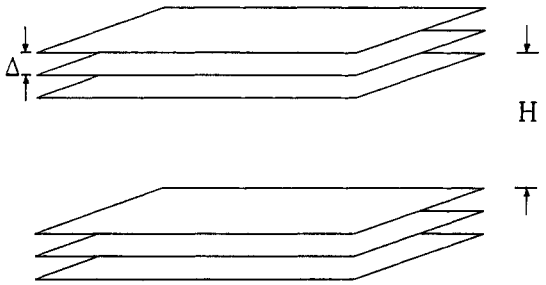

Figure 1. The carbon slit pore model.

model of the structure of a fluid confined in a pore, as has been confirmed by comparison to computer simulation studies.[20] From the model isotherms predicted by nonlocal theory, we then calculate the PSDs of several porous carbons by solving for the distribution function in eq 5.

2.2. Description of the Model. To model nitrogen adsorption on activated carbon, we select a slit pore geometry for the individual pores, as suggested by the sieving properties of microporous carbons.[7] The individual pore is represented as two semi-infinite parallel graphitic slabs separated by a physical width H, the distance between the centers of the surface carbon atoms (Figure 1). The graphite layers in each slab are separated by a uniform spacing Δ. By using infinite boundaries in the lateral directions, we are implicitly assuming that the aspect ratio of pore length to pore width is large. Thus we neglect the influence of connectivity in the pore model. We further assume that the graphite surface is smooth and rigid and that no surface functional groups are present. This eliminates the effects of corrugation, swelling, and chemical heterogeneity. For the fluid–fluid interaction potential ϕ_{ff}, we use the Lennard-Jones 12-6 pair potential

$$\phi_{ff}(r) = 4\epsilon_{ff}\left[\left(\frac{\sigma_{ff}}{r}\right)^{12} - \left(\frac{\sigma_{ff}}{r}\right)^{6}\right] \quad (6)$$

where r is the separation distance and ϵ_{ff} and σ_{ff} are fitted parameters for the bulk nitrogen well depth and molecular diameter. The solid–fluid interaction potential ϕ_{sf} for nitrogen interacting with a single graphitic slab is well described by the Steele 10-4-3 potential[21]

$$\phi_{sf}(z) = 2\pi\epsilon_{sf}\rho_s\sigma_{sf}^2\Delta\left[\frac{2}{5}\left(\frac{\sigma_{sf}}{z}\right)^{10} - \left(\frac{\sigma_{sf}}{z}\right)^{4} - \frac{\sigma_{sf}^4}{3\Delta(z+0.61\Delta)^3}\right] \quad (7)$$

where z is the distance from the graphite surface, ρ_s is the solid density, and ϵ_{sf} and σ_{sf} are fitted parameters for the nitrogen–carbon well depth and effective diameter. The 10-4-3 potential is obtained by integrating the Lennard-Jones potential between one fluid molecule and each carbon atom of the individual graphite planes. The "10" and "4" terms represent the repulsive and attractive interactions of the fluid molecule with the surface graphitic plane, while the "3" term results from the summation of the attractive part of the potential over the remaining layers of the solid. (The repulsive interactions of the fluid molecule with the subsurface graphite planes are small and therefore neglected.) For a slit pore, the fluid molecule will interact with both graphite slabs; hence, the full external potential V_{ext} is written as

$$V_{ext}(z) = \phi_{sf}(z) + \phi_{sf}(H - z) \quad (8)$$

In eq 7 we fix $\rho_s = 0.114$ Å^{-3} and $\Delta = 3.35$ Å.[21] Equations 6 and 7 thus each contain two parameters (σ_{ff}, ϵ_{ff}; σ_{sf}, ϵ_{sf}) that must be fitted to experimental observations. To ensure that the fit is as realistic as possible, we select experimental data that reflect the conditions under which the nitrogen adsorption isotherms of the porous carbons were measured. Hence, using the density functional theory model outlined in section 2.3, we fit the fluid–fluid potential parameters so that the model reproduces the bulk nitrogen saturated liquid density[22] of 0.02887 mol cm^{-3} and saturation pressure of 1 atm at the normal boiling point of 77.347 K, the temperature at which all of the experimental isotherms were measured.

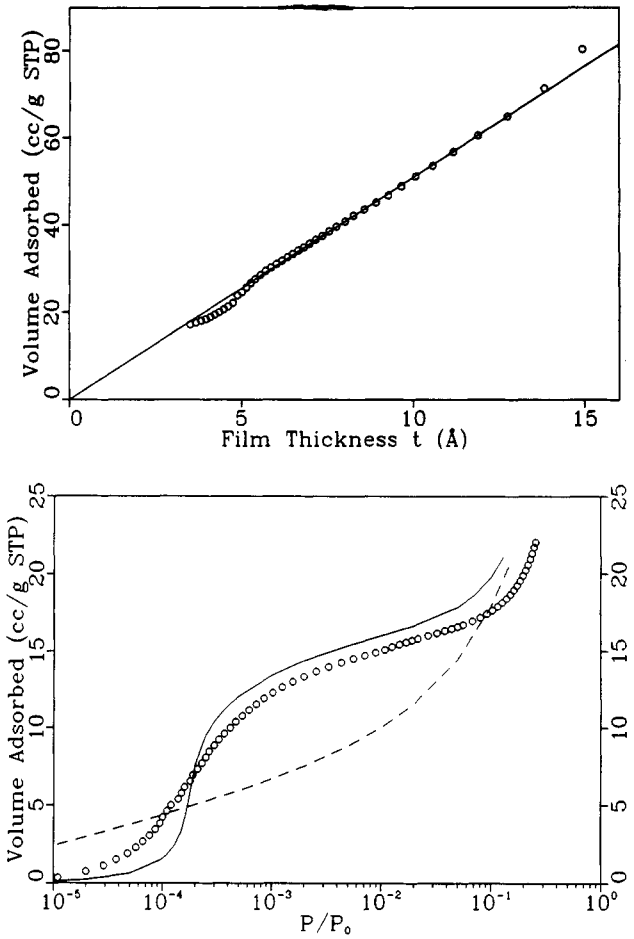

Figure 2. Nonporous Vulcan isotherm, nitrogen on carbon at 77 K. (a, top) Surface area determination of Vulcan sorbent using the method of deBoer et al.[23] The volumetric uptake is plotted against the universal t-curve at corresponding pressures. The slope of the linear region is the specific surface area. (b, bottom) Comparison of theoretical and experimental nonporous isotherms: dashed line, local theory; solid line, nonlocal theory; symbols, experimental Vulcan isotherm.

The solid–fluid parameters are chosen to provide the best fit possible to the experimental measurement of nitrogen adsorption on the nonporous carbon Vulcan at 77.347 K. Theory predicts the adsorbed volume of nitrogen per unit area of pore surface. In order to convert this quantity into the theoretical adsorption on Vulcan, the surface area of the real material must be known. In the present work this has been determined using de Boer's method[23] of scaling the experimental data to the "universal" t-curve at high pressures ($P/P_0 \geq 0.3$), as shown in Figure 2a. In this way a specific surface area of 78.6 m^2/g was obtained for Vulcan.

The best fits to the nonporous isotherm obtained by using theory (Figure 2b) are given at this value of the surface area. The nonlocal theory is a good approximation over several decades of pressure, especially in the middle range that is of importance for adsorption in microporous materials. The fluid–fluid and solid–fluid potential parameters are summarized in Table II for both versions of the density functional theory.

It is significant that it was not possible to simultaneously fit both the low-pressure ($P/P_0 \leq 0.1$) and high-pressure ($P/P_0 \geq 0.1$) adsorption on Vulcan using an effective Lennard-Jones atomic

TABLE II: Interaction Potential Parameters of Density Functional Theory Model

parameter	local theory	nonlocal theory
σ_{ff} (Å)	3.572	3.572
ϵ_{ff}/k (K)	93.98	93.98
σ_{sf} (Å)	3.494	3.494
ϵ_{sf}/k (K)	74.23	53.22

potential for nitrogen. One possible reason is that the adsorption at low pressures is affected by the anisotropy of the nitrogen molecule and its quadrupolar interaction with the graphitic surface. These features are not explicitly present in the current model but will be incorporated into future work.

To model the overall sorbent structure, we envision an array of noninteracting individual slit pores whose distribution of pore widths can be described by a function $f(H)$. Clearly, we must select a distribution function that is nonnegative for all pore widths H. We also assume that $f(H)$ is continuous. Two functions which satisfy these conditions are the gamma distribution

$$f(H) = \sum_{i=1}^{m} \frac{\alpha_i(\gamma_i H)^{\beta_i}}{\Gamma(\beta_i)H} \exp(-\gamma_i H) \tag{9}$$

and the log normal distribution

$$f(H) = \sum_{i=1}^{m} \frac{\alpha_i}{\gamma_i H(2\pi)^{1/2}} \exp\left(\frac{-[\ln(H) - \beta_i]^2}{2\gamma_i^2}\right) \tag{10}$$

In equations 9 and 10, m is the number of modes of the distribution, and α_i, β_i, and γ_i are adjustable parameters that define the amplitude, mean, and variance of mode i. The equations are used to represent the PSD in the fitting of eq 5. In section 4 the choice of PSD function is discussed at greater length. For now, we turn to the development of the density functional theory model of adsorption.

2.3. Derivation of the Governing Equations. Each individual slit pore has a fixed geometry and is open and in contact with the bulk fluid (nitrogen). The temperature is fixed at the nitrogen boiling point. For this system, the grand canonical ensemble provides an appropriate description of the thermodynamics. In this ensemble, the chemical potential μ, temperature T, and pore volume V are specified. The starting point of our derivation is therefore the grand potential functional. For a fluid in the presence of a spatially varying external potential $V_{ext}(\mathbf{r})$, the grand potential functional Ω can be written as

$$\Omega[\rho_L(\mathbf{r})] = F[\rho_L(\mathbf{r})] - \int d\mathbf{r}\, \rho_L(\mathbf{r})[\mu - V_{ext}(\mathbf{r})] \tag{11}$$

where F is the intrinsic Helmholtz free energy functional, ρ_L is the local fluid density at position $\mathbf{r}$, and the integration is performed over V. We expand F in a perturbative fashion about a reference system of hard spheres of diameter d

$$F[\rho_L(\mathbf{r})] = F_h[\rho_L(\mathbf{r});d] + \frac{1}{2}\int\int d\mathbf{r}\, d\mathbf{r}'\, \rho_L^{(2)}(\mathbf{r},\mathbf{r}')\phi_{att}(|\mathbf{r}-\mathbf{r}'|) \tag{12}$$

where F_h is the hard sphere Helmholtz free energy functional, $\rho_L^{(2)}$ is the pair distribution function, and ϕ_{att} is the attractive portion of the fluid–fluid potential. If we now invoke the mean field approximation, whereby correlations due to attractive forces are neglected, we obtain the mean field theory result

$$F[\rho_L(\mathbf{r})] = F_h[\rho_L(\mathbf{r});d] + \frac{1}{2}\int\int d\mathbf{r}\, d\mathbf{r}'\, \rho_L(\mathbf{r})\rho_L(\mathbf{r}')\phi_{att}(|\mathbf{r}-\mathbf{r}'|) \tag{13}$$

The attractive part of the fluid–fluid potential is represented by the WCA form of the Lennard-Jones potential

$$\begin{aligned}\phi_{att}(|\mathbf{r}-\mathbf{r}'|) &= \phi_{ff}(|\mathbf{r}-\mathbf{r}'|), \quad &|\mathbf{r}-\mathbf{r}'| > r_m \\ &= -\epsilon_{ff}, \quad &|\mathbf{r}-\mathbf{r}'| < r_m\end{aligned} \tag{14}$$

where $r_m = 2^{1/6}\sigma_{ff}$ is the separation at which the Lennard-Jones potential attains its minimum. The hard sphere term F_h is further divided into an ideal gas component F_{id} and an excess component F_{ex}

$$F_h[\rho_L(\mathbf{r});d] = F_{id}[\rho_L(\mathbf{r})] + F_{ex}[\rho_L(\mathbf{r});d] \tag{15}$$

The ideal contribution is exactly local (i.e. F_{id} at $\mathbf{r}$ depends only on ρ_L at $\mathbf{r}$) and is given by

$$F_{id}[\rho_L(\mathbf{r})] = kT\int d\mathbf{r}\, \rho_L(\mathbf{r})[\ln(\Lambda^3\rho_L(\mathbf{r})) - 1] \tag{16}$$

where $\Lambda = h/(2\pi mkT)^{1/2}$ is the thermal deBroglie wavelength, h is the Planck constant, k is the Boltzmann constant, and m is the molecular mass of nitrogen. The excess term is

$$F_{ex}[\rho_L(\mathbf{r});d] = kT\int d\mathbf{r}\, \rho_L(\mathbf{r})f_{ex}[\bar{\rho}(\mathbf{r});d] \tag{17}$$

where f_{ex} is the excess Helmholtz free energy per molecule:

$$f_{ex}[\bar{\rho}(\mathbf{r});d] = \mu_h[\bar{\rho}(\mathbf{r});d] - \frac{P_h[\bar{\rho}(\mathbf{r});d]}{\bar{\rho}(\mathbf{r})} - kT[\ln(\Lambda^3\bar{\rho}(\mathbf{r})) - 1] \tag{18}$$

In the preceding equation, μ_h and P_h are the chemical potential and pressure, respectively, of a uniform hard sphere fluid and $\bar{\rho}$ is a smoothed density which is defined as

$$\bar{\rho}(\mathbf{r}) = \int d\mathbf{r}'\, \rho_L(\mathbf{r}')w[|\mathbf{r}-\mathbf{r}'|;\bar{\rho}(\mathbf{r})] \tag{19}$$

The choice of the weighting function w depends on the version of density functional theory used. In the local density approximation, the hard sphere excess free energy is evaluated using the local density profile of the fluid. For this approximation, the weighting function is simply the delta function

$$w_{loc}[|\mathbf{r}-\mathbf{r}'|;\bar{\rho}(\mathbf{r})] = \delta(|\mathbf{r}-\mathbf{r}'|) \tag{20}$$

In the smoothed (nonlocal) density approximation, the weighting function is chosen to give a good description of the hard sphere direct pair correlation function for the uniform fluid over a wide range of densities. Several types of weighting functions have been proposed to study fluids confined in pores (see Evans[24] for a review). In this work we use Tarazona's model for the smoothing functions.[25] This model has been shown to give good agreement with simulation results for the density profile and surface tension of hard sphere fluids near hard walls and Lennard-Jones fluids near Lennard-Jones walls. The Tarazona prescription for the weighting functions uses a power series expansion in the smoothed density. Truncating the expansion at second order yields

$$w_{nonloc}[|\mathbf{r}-\mathbf{r}'|;\bar{\rho}(\mathbf{r})] = w_0(|\mathbf{r}-\mathbf{r}'|) + w_1(|\mathbf{r}-\mathbf{r}'|)\bar{\rho}(\mathbf{r}) + w_2(|\mathbf{r}-\mathbf{r}'|)\bar{\rho}(\mathbf{r})^2 \tag{21}$$

The expansion coefficients w_0, w_1, and w_2 are reported elsewhere.[25] To calculate the hard sphere excess free energy, we use the Carnahan–Starling equation of state[26]

$$P_{hs}[\bar{\rho}] = \bar{\rho}kT\frac{1 + \bar{\xi} + \bar{\xi}^2 - \bar{\xi}^3}{(1-\bar{\xi})^3} \tag{22}$$

$$\mu_{hs}[\bar{\rho}] = kT\left[\ln(\Lambda^3\bar{\rho}) + \frac{8\bar{\xi} - 9\bar{\xi}^2 + 3\bar{\xi}^3}{(1-\bar{\xi})^3}\right] \tag{23}$$

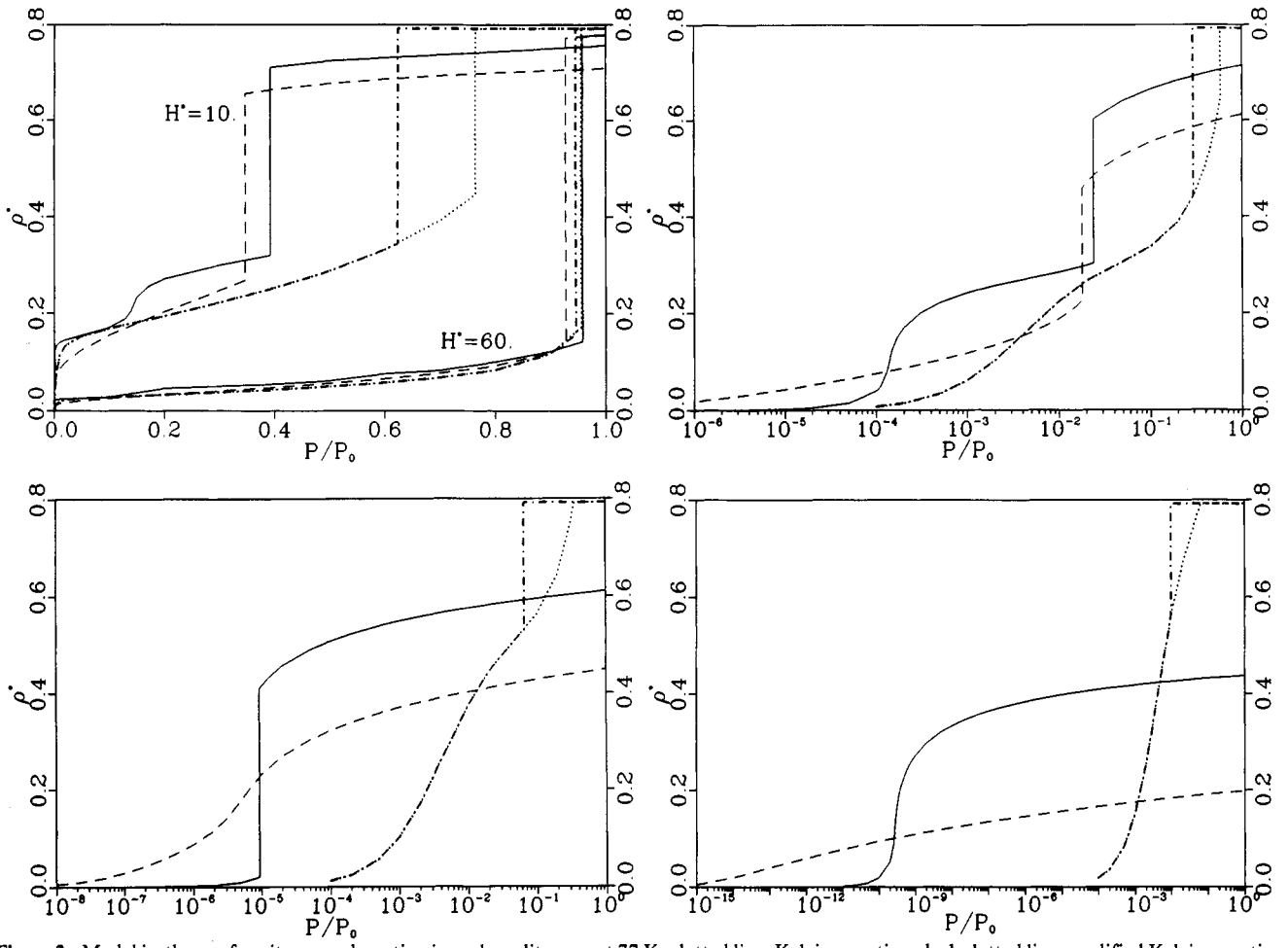

Figure 3. Model isotherms for nitrogen adsorption in carbon slit pores at 77 K: dotted line, Kelvin equation; dash-dotted line, modified Kelvin equation; dashed line, local theory; solid line, nonlocal theory. Pore widths: (a, top left) $H^* = 60$ and $H^* = 10$; (b, top right) $H^* = 5$; (c, bottom left) $H^* = 3$; (d, bottom right) $H^* = 2$.

where

$$\bar{\xi} = \frac{\pi}{6}\bar{\rho}d^3 \tag{24}$$

The equivalent hard sphere diameter, d, is calculated as a function of temperature. The explicit form approximates the Barker–Henderson diameter[27]

$$\frac{d}{\sigma_{ff}} = \frac{\eta_1 kT/\epsilon_{ff} + \eta_2}{\eta_3 kT/\epsilon_{ff} + \eta_4} \tag{25}$$

where the constants, η_i, are chosen to give good agreement between theory and simulation at low temperatures.[28] In this work we use $\eta_1 = 0.3837$, $\eta_2 = 1.035$, $\eta_3 = 0.4249$, and $\eta_4 = 1$. To solve for the equilibrium density profile, the grand potential functional of eq 11 is minimized with respect to density

$$\left.\frac{\delta\Omega[\rho_L(\mathbf{r})]}{\delta\rho_L(\mathbf{r})}\right|_{\rho_L=\rho_{L,eq}} = 0 \tag{26}$$

For large pores, two minimum density profiles commonly arise. These are the liquid and vapor branches associated with thermodynamic hysteresis in individual slit pores. When more than one minimum exists, the density profile which has the lower grand potential energy is the stable branch. The chemical potential at which condensation occurs is the value for which the two minima have the same grand potential energy.

For the model described in section 2.2, the density profile will be one dimensional; that is, the density varies in the z direction only. A numerical iteration scheme is used to solve eq 26 for $\rho_L(z)$ over a range of chemical potentials μ for selected values of H. The chemical potential can be related to the bulk reduced pressure P/P_0 through the bulk fluid equation of state. The mean pore fluid density ρ is calculated according to

$$\rho = \frac{1}{H}\int_0^H \rho_L(z)\,dz \tag{27}$$

Thus, using density functional theory, the set of model isotherms $\rho(P,H)$ is generated for use in eq 5.

It is convenient to scale the pore width and mean fluid density with respect to the fluid–fluid molecular diameter. In subsequent sections, we use the following scalings:

$$H^* = H/\sigma_{ff} \qquad \rho^* = \rho\sigma_{ff}^3$$

3. Density Functional Theory: Model Isotherms

3.1. Comparison of Theoretical Methods. In Figure 3, we compare the model isotherms generated from local and nonlocal theory and from the Kelvin and modified Kelvin equations for adsorption in a selection of pore widths at 77 K. The condensation pressures of the Kelvin and modified Kelvin equations are calculated from eqs 1 and 2, respectively, with $\gamma_l = 8.88$ mN m^{-1} for nitrogen[12] and with $n = 2$ substituted in eq 2. To estimate the fluid density in the pore below the condensation pressure, we use the Cranston–Inkley method[2]

$$\rho(P/P_0) = \rho_b(P/P_0) + \frac{2\rho_l t(P/P_0)}{H} \tag{28}$$

where ρ_b is the bulk nitrogen density, ρ_l is the saturated liquid nitrogen density (assumed here to be equal to the adsorbed film density), and t is the universal isotherm or "t-curve" of nitrogen adsorption on nonporous carbon. Hence, we use standard film

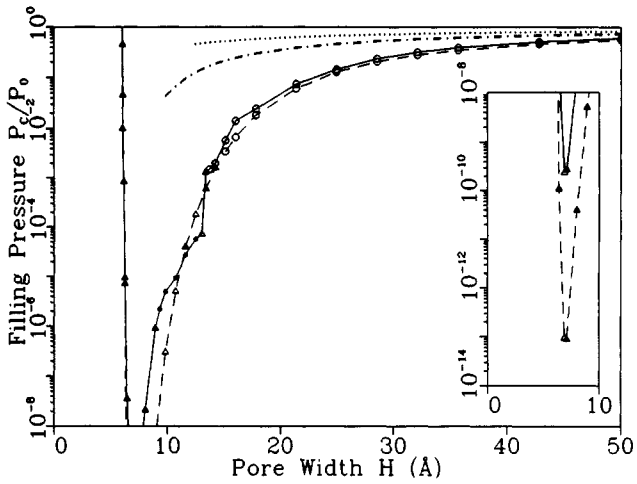

Figure 4. Pore filling pressures for nitrogen in porous carbon, 77 K: dotted line, Kelvin equation; dash-dotted line, modified Kelvin equation; dashed line, local theory; solid line, nonlocal theory. Open circles denote capillary condensation, filled circles indicate a 0 → 1 layering transition, and triangles denote continuous filling of pores. The inset shows the low pressure filling region of the ultramicropores, predicted by local and nonlocal theory.

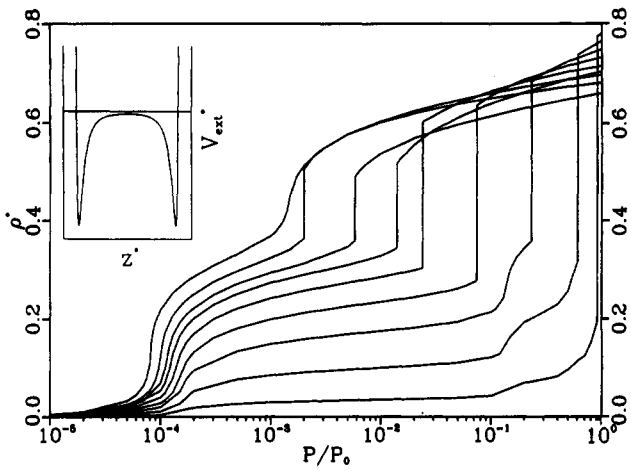

Figure 5. Nonlocal theory isotherms for nitrogen adsorbed in NLT mesoporous carbon slits at 77 K. The pore widths, reading from left to right, are H^* = 3.75, 4, 4.25, 4.5, 5, 6, 8, 14, and 40. The isotherm at H^* = 3.75 shows the onset of the continuous filling band (NLT Supermicropores A). The inset shows the characteristic solid–fluid potential profile of the mesopore-sized slits.

thickness data to calculate the fluid density in the Kelvin-type models. Above the condensation pressure, the fluid density is set equal to the bulk saturated liquid nitrogen density. In Figure 3a we observe that the Kelvin equation and its modified form predict the condensation pressures of the largest pores satisfactorily, but in Figure 3b–d they overestimate by orders of magnitude the filling pressures of micropores. Indeed, even for the moderately-sized mesopore H^* = 10, the Kelvin equation and modified Kelvin equation overestimate the nonlocal theory condensation pressure by approximately 100% and 60%, respectively. Although the modified Kelvin equation offers a modest improvement over its parent equation, it is clear that such adjustments are insufficient to correct the deficiencies of classical modeling at the micropore level.

The local density functional theory isotherms are a marked improvement over the Kelvin-type counterparts and agree qualitatively with the nonlocal theory isotherms for the mesopore-sized slits. When applied to the micropores, the local theory results begin to diverge, as the errors in the modeling of the local density at the solid-fluid interface become progressively larger. For the ultramicropores (Figure 3c,d), local theory greatly overestimates the uptake of nitrogen at low pressures. By contrast, the filling pressures and adsorption isotherms predicted by nonlocal theory were found to be in excellent agreement with Gibbs ensemble Monte Carlo simulation results for both carbon mesopores and micropores in a recent study.[20]

The difference in the local and nonlocal theory filling pressures can be understood by comparing the adsorbed fluid density profiles predicted by the two theories. The use of the smoothed density in nonlocal theory produces the sharply oscillating density profile expected of a fluid adjacent to a solid surface, as observed in computer simulations[20] and in surface force measurements.[29] The local theory density profile, however, is comparatively unstructured. Because the local excess free energy density in eq 18 is evaluated as the free energy of an equivalent homogeneous bulk fluid of the same local density, the local theory will not predict a large peak in the monolayer density, as this would result in an unrealistically large value of the free energy. Instead, the local theory profile is relatively smooth, with only a modest peak in the monolayer. This deficiency is most apparent when local theory is applied to modeling adsorption in the micropores, in which the gradients in the density profile are most pronounced.

In Figure 4, the filling pressures are plotted versus pore width for each of the four models considered. For pores which fill continuously, the filling pressure is estimated from the inflection point in the isotherm. As noted previously, the overlap of the wall potentials results in a deep minimum in the filling pressures of the ultramicropores. From the nonlocal theory coexistence curve, one discerns a minimum filling pressure of $P_{min}/P_0 = 10^{-10}$. This provides a guide to the minimum pressure required to determine experimentally the full range of condensation/filling behavior in all pore sizes. There are several additional features of interest in the nonlocal theory isotherms; these are discussed in section 3.2.

3.2. Nonlocal Theory Isotherms. Individual pore isotherms were generated using nonlocal theory (NLT) for a range of pore sizes from H^* = 1.68 to 100 (6 to 360 Å) at T = 77 K. The nitrogen adsorption isotherms in carbon mesopores are shown in Figure 5. Pores of this size range, which we shall denote NLT mesopores, exhibit type IV behavior in the IUPAC classification scheme.[1] At low pressures, the monolayer is formed; as the pressure is increased, additional multilayers are adsorbed, until the condensation pressure is reached, whereupon the phase transition to the liquid state occurs. Above the condensation pressure, there is a gradual increase in the mean density due to the compression of the nitrogen in the liquid-filled pore. As the pore width is reduced, the condensation pressure also decreases (see Figure 5). This is explained by considering the solid–fluid slit potential. As the slit walls move closer together, the bulklike region in the center of the pore, where V_{ext} is approximately zero, disappears, and adsorption is enhanced throughout the pore. Additionally, the proximity of adsorbed fluid layers on opposing walls increases fluid–fluid interactions, further promoting adsorption of multilayers. A transition from capillary condensation to continuous filling occurs at a critical width of H_{c1}^* = 3.8, or 13.6 Å (see Figure 5). This critical width is slightly smaller than the local theory transition width of H^* = 4 (14.3 Å).

Interestingly, there is a second region of discontinuous pore filling in the nonlocal theory isotherms, separate from the capillary condensation region, at pore widths below H_{c1}^*. This regime is shown in Figure 6. A narrow band of continuously filling slits exists between H_{c2}^* = 3.6 and H_{c1}^* = 3.8 (12.8–13.6 Å); we denote these the NLT supermicropores A. For larger pores (the NLT mesopores), one observes condensation in the multilayer; for the range of pore widths from H_{c3}^* = 2.55 to H_{c2}^* = 3.6, or 9.1 to 12.8 Å (Figure 6), a layering transition occurs wherein the incomplete monolayer on each pore wall abruptly fills to completion. The behavior of these pores, which we shall denote the NLT supermicropores B, is absent from the local theory results.

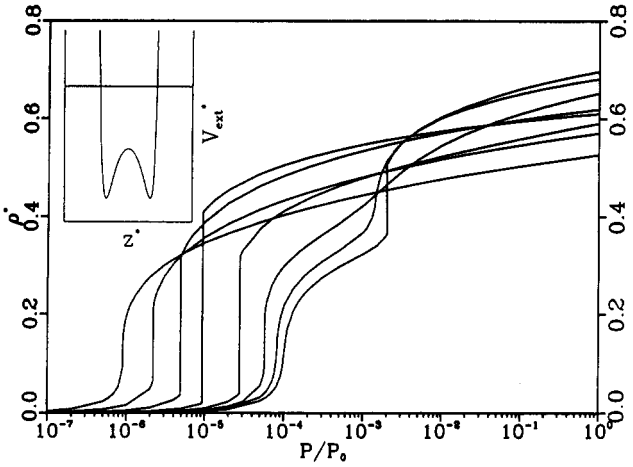

Figure 6. Nonlocal theory isotherms for nitrogen adsorbed in NLT supermicroporous carbon slits at 77 K. The pore widths, reading from left to right, are $H^* = 2.5, 2.6, 2.75, 3, 3{,}25, 3.5, 3.75$, and 4. The narrow band of pore widths from approximately $H^* = 3.6$ to 3.8 (NLT supermicropores A) fill continuously. Larger pores undergo capillary condensation (see Figure 5). Pores with widths between $H^* = 2.55$ and 3.6 (NLT supermicropores B) exhibit a $0 \rightarrow 1$ layering transition. The inset shows the characteristic solid–fluid potential profile of the supermicropore-sized slits.

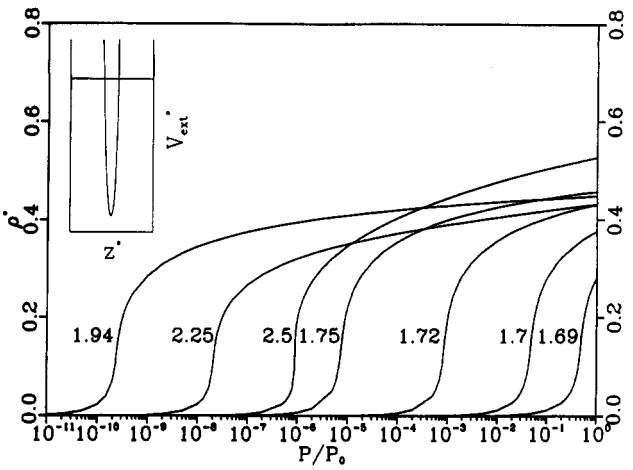

Figure 7. Nonlocal theory isotherms for nitrogen on carbon in NLT ultramicropores. Reading from left to right: $H^* = 1.94, 2.25, 2.5, 1.75, 1.72, 1.7$, and 1.69. The filling pressures of the pores from $H^* = 2.5$ to 1.94 (NLT ultramicropores A) are greatly reduced due to the coalescence of the solid–fluid potential minima. The minimum filling pressure occurs at $H^* = 1.94$, where the solid–fluid potential enhancement is maximized. Pores smaller than $H^* = 1.94$ (NLT ultramicropores B) show a rapid rise in filling pressure with decreasing size due to repulsive potential overlap. For pores of widths $H^* = 1.68$ or smaller, nitrogen uptake is essentially zero at or below the saturation pressure. The inset shows the characteristic solid–fluid potential profile of the ultramicropore-sized slits.

For single carbon surfaces, both experimental and simulation studies have shown that $0 \rightarrow 1$ layering transitions occur at temperatures well below the temperature of 77 K studied here. Thus, for large carbon pores, the critical temperature for this transition lies below 77 K, but for sufficiently small pores the critical temperature rises above this value. We believe this transition in the supermicropores arises from a cooperative adsorption process, where the proximity of the absorbed films on each wall (Figure 6) enables an energetically favorable phase transition, as opposed to the usual continuous filling of the monolayer. The continuous filling band of NLT supermicropores A seems to result from the nonintegral reduced slit widths of this set. Hence, the gap between the adsorbed films is too large to permit cooperative adsorption in the monolayer and too small to allow a phase transition in the multilayer. The effect of nonintegral pore width also causes oscillations in the density of the liquid-filled pore at the bulk saturation pressure, due to inefficient packing of the nitrogen molecules in the multilayer. For still smaller pore widths (H^* below H_{c3}^*), we observe a return to continuous filling (Figure 7). Pores in the size range between $H^* = 1.94$ and 2.55 (6.9 and 9.1 Å), which we denote NLT ultramicropores A, are so narrow that only a single complete layer of molecules can be accommodated. The isotherms resemble the IUPAC type I isotherm characteristic of micropore adsorption.[1] As shown in Figure 7, the double minima of the solid–fluid potential coalesces at a pore width of $H^* = 2.25$ (8.0 Å). This results in an enhancement of the potential well strength, which is maximized to roughly double its original depth at $H^* = 1.94$ (6.9 Å). A corresponding reduction in the filling pressures is seen, with the minimum (at $H^* = 1.94$) occurring at approximately $P/P_0 = 10^{-10}$, a pressure on the order of 0.1 μTorr. As the pore width is reduced beyond this minimum, the repulsive parts of the opposing wall potentials begin to overlap, until the entire solid–fluid slit potential becomes repulsive. Hence, there is a rapid rise in filling pressures as the pore width drops below $H^* = 1.94$; we call these pores the NLT ultramicropores B. For pores with physical width narrower than $H^* = 1.69$ (6.0 Å), the pore space is inaccessible to nitrogen and no adsorption occurs. It is notable that adsorption in the ultramicropores is considerably reduced due to exclusion of the fluid molecules from the region near the slit walls. Only in the large NLT mesopores (Figure 5) does the mean density in the pore approach the bulk saturated liquid value of $\rho^* = 0.792$.

We summarize our classification of the nonlocal theory model adsorption isotherms in Table III. While the IUPAC designation of pore sizes (Table I) is a helpful guide to anticipating filling behavior, it is evident from the results presented here that the type of adsorption depends as much upon the adsorbate characteristics as it does upon the structure of the adsorbent. Therefore, it is perhaps more relevant to use a classification scheme incorporating a pore size scaled with respect to the fluid molecular diameter, as shown in Table III (see also Balbuena and Gubbins[30]).

4. PSD Interpretation of Porous Carbons

4.1. Comparison of Theoretical PSD Results. To determine the PSDs of porous carbons from experimental nitrogen adsorption data, the set of model isotherms presented in section 3.2 is correlated as a function of pressure and pore width. We then solve the integral of eq 5 numerically, inserting one of the model distributions of eqs 9 and 10 and employing a simple minimization algorithm to optimize the set of parameters α_i, β_i, γ_i of the PSD function. A least-squares error minimization criterion is used to determine the optimum fit

$$E = \frac{1}{n_P}\sum_{i=1}^{n_P}\left[\sum_{j=1}^{n_H}\rho(P_i,H_j)f(H_j)\Delta H_j - N(P_i)\right]^2 \qquad (29)$$

where E is the mean square error per fitted point, n_P is the number of points on the isotherm, and n_H is the number of width subintervals in the numerical integration. The choice of the number of modes in the PSD function is arbitrary, provided that enough are used to give $f(H)$ sufficient flexibility. In practice, however, the number of inflection points in the experimental isotherm can be used as an estimate of the number of modes required to yield an acceptable fit. We make this assertion on the basis of the one-to-one correspondence of filling pressure to pore width in the nonlocal theory results of Figure 4 (excluding the NLT ultramicropores B). All PSD results that follow were obtained by using a trimodal gamma distribution, except where otherwise noted.

The PSDs of three carbons have been fitted using this method. The standard pretreatment for all of the samples was a bakeout at 300 °C for 16 h at 10^{-6} Torr. The nitrogen uptake data were

TABLE III: Classification of Carbon Slit Pore Widths According to the Nonlocal Theory (NLT) Description

class	scaled width H*	width H(Å)	pore potential	type of filling
NLT Mesopore	≥ 3.8	≥ 13.6	double minimum, bulklike interior	capillary condensation
NLT Supermicropore A	3.6–3.8	12.8–13.6	double minimum, attractive interior	continuous filling
NLT Supermicropore B	2.55–3.6	9.1–12.8	double minimum, attractive interior	0 → 1 layering
NLT Ultramicropore A	1.94–2.55	6.9–9.1	single minimum, attractive overlap	continuous filling
NLT Ultramicropore B	≤ 1.94	≤ 6.9	single minimum, repulsive overlap	continuous filling

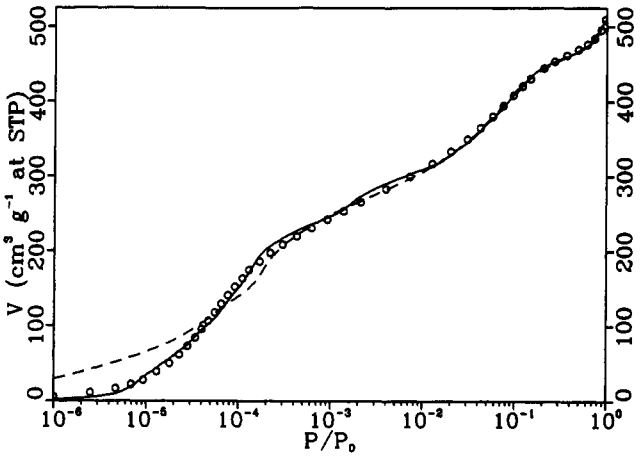

Figure 8. Nitrogen adsorption on microporous carbon AC610 at 77 K: symbols, experimental uptake measurement; solid line, nonlocal theory fitted isotherm; dashed line, local theory fitted isotherm.

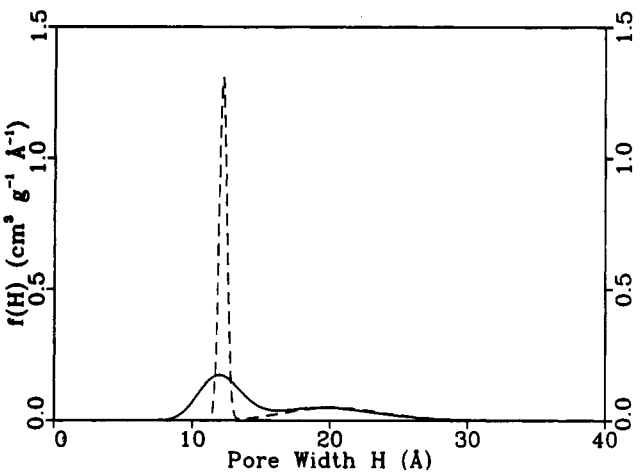

Figure 9. Pore size distribution for carbon AC610: solid line, nonlocal theory; dashed line, local theory.

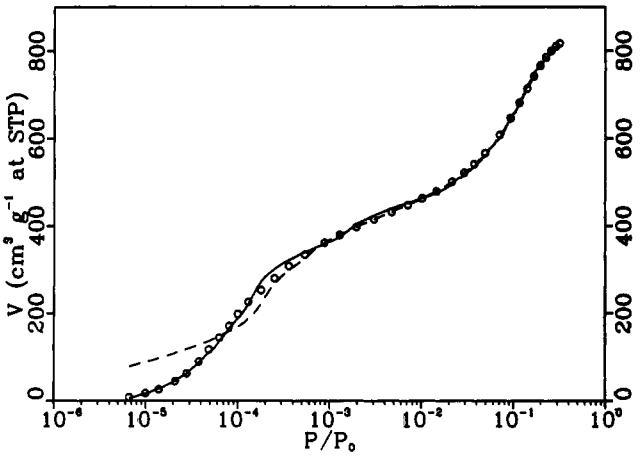

Figure 10. Nitrogen adsorption on microporous carbon AX21 at 77 K: symbols, experimental uptake measurement; solid line, nonlocal theory fitted isotherm; dashed line, local theory fitted isotherm.

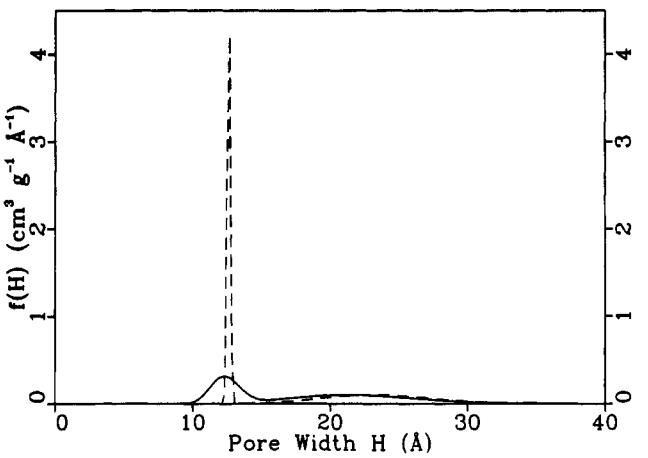

Figure 11. Pore size distribution for carbon AX21: solid line, nonlocal theory; dashed line, local theory.

collected by static flow measurement on a Coulter Omnisorp. In Figure 8 we show the adsorption isotherm of a highly microporous carbon, AC610. It is observed that the nonlocal theory gives a good fit to the full pressure range of the experimental isotherm, whereas the local theory overestimates the adsorption at low pressures. The PSDs which correspond to these isotherm fits are displayed in Figure 9. The local theory PSD overestimates the height of the micropore peak relative to the nonlocal PSD. This is a consequence of the limitations of local theory at small pore widths (see Figure 3).

In Figures 10 and 11 we show the adsorption isotherm and PSD predictions for AX21, another microporous carbon. The AX21 fits were obtained by using a bimodal gamma distribution. As in the case of AC610, the local theory tends to minimize the peak width in order to reduce the error in the low pressure fit to the isotherm. The improvement in the accuracy of the PSD results using nonlocal theory again demonstrates the advantage of the nonlocal model. For both AC610 and AX21 the nonlocal theory isotherm and the experimental isotherm are in excellent agreement.

Finally, in Figure 12 we present the experimental isotherm and theoretical fits for carbon CXV, which has a combination of microporosity and mesoporosity. The corresponding PSDs are given in Figure 13. For this carbon the Kelvin and modified Kelvin equation fits are also shown. It is seen that the Kelvin-type models perform very poorly, yielding predictions of unphysical pore widths. The local theory fits the experimental isotherm more closely, but the local theory PSD is known to overestimate the height of the micropore peak. The nonlocal theory isotherm is in reasonable agreement with the experimental data, although there is some deviation around $P/P_0 = 10^{-4}$. For the present version of nonlocal theory used, it is not possible to reproduce the large uptake near the saturation pressure without slightly overestimating the uptake at the monolayer filling pressure. It is known that density functional theory predicts a higher bulk fluid critical temperature than found from comparable Lennard-Jones molecular simulations. Therefore, at subcritical temperatures, the nonlocal theory may exhibit too sharp a rise in the isotherm at the monolayer pressure, as is seen in Figure 12. A second possibility, mentioned in section 2.2, is that the neglected quadrupole and the nonspherical shape of the nitrogen molecule may affect the shape of the isotherm at $P/P_0 = 10^{-4}$. Nonetheless, since nonlocal theory gives the most accurate description of micropore filling, the nonlocal PSD results are the most reliable interpretation.

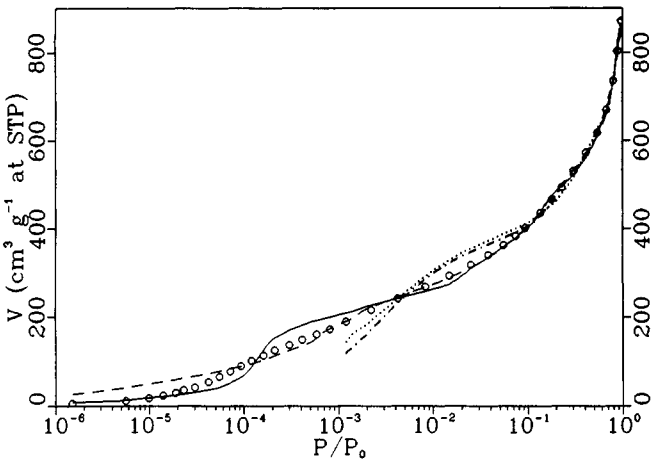

Figure 12. Nitrogen adsorption on meso/microporous carbon CXV at 77 K: symbols, experimental uptake measurement. Lines show fitted isotherms: solid line, nonlocal theory; dashed line, local theory; dotted line, Kelvin equation; dash-dotted line, modified Kelvin equation.

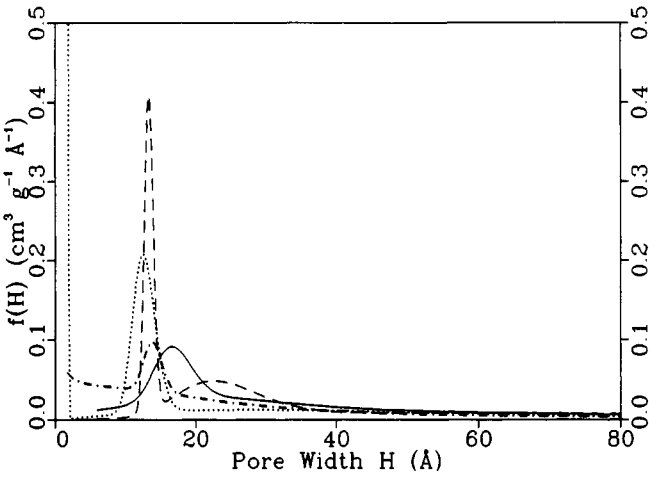

Figure 13. Pore size distribution for carbon CXV: solid line, nonlocal theory; dashed line, local theory; dotted line, Kelvin equation; dash-dotted line, modified Kelvin equation.

4.2. Limitations of the PSD Analysis Method. If we accept the model represented by eq 5, inspection of this equation indicates that there are three possible sources of error in the PSD calculation: (1) the reliability of the experimental uptake data $N(P)$; (2) the accuracy of the model adsorption isotherms $\rho(P,H)$; (3) the mathematical uncertainties associated with the selection of the PSD function $f(H)$ and the solution of the adsorption integral. We shall consider each of these possibilities in turn.

Experimental Limitations. As noted in section 3.1, the characterization of strongly adsorbing materials such as carbons requires careful measurement of the low pressure isotherm. If such pressures cannot be attained, the PSD calculation must necessarily be truncated at the experimentally imposed lower bound. We emphasize that during the fitting procedure, the full range of pore widths is employed in the calculations, since changes in the density of the liquid-filled micropores contribute to the overall isotherm. It is only after the optimum PSD is determined that the distribution is truncated.

For porous graphitic carbon, the theoretical calculations suggest that the minimum filling pressure is approximately 10^{-10} P_0, or 10^{-7} Torr. The experimental isotherms presented in this work sample pressures as low as 10^{-6} P_0, so a portion of the ultramicropore range is not accessible to these measurements.

When calculating PSDs for microporous sorbents such as AX21 or AC610, it is important to allow for kinetic limitations in the adsorption measurement due to the slow rates of diffusion through

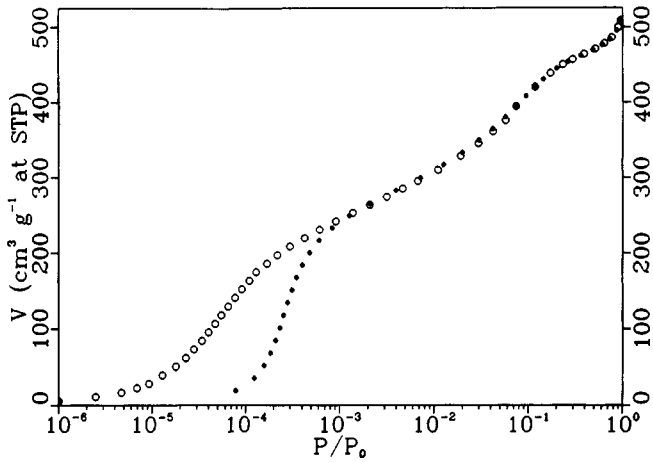

Figure 14. Comparison of static and flow uptake measurements of nitrogen on carbon AC610 at 77 K: open circles, static measurement; filled circles, flow measurement.

the narrow pores. As an example, a comparison of the experimental uptake of nitrogen on carbon AC610 using a static and a flow measurement is shown in Figure 14. The adsorption at low pressure is markedly enhanced in the static experiment, since the diffusion-limited micropores fill at these pressures. The implication is that improperly equilibrated flow adsorption measurements will produce PSDs that underestimate the population of micropores in the sorbent.

We note finally that for all of the PSD fitting we use only the adsorption branch of the experimental isotherm. We avoid fitting the desorption branch, as there may be hysteresis effects in this branch associated with pore blocking due to the connectivity of the pore structure. Network hysteresis, which has been studied by several workers[31,32,33] using percolation theory methods, is commonly observed in mesoporous sorbents. Pore blocking moves the desorption branch to an emptying pressure below that of the adsorption pressure; consequently, fitting the PSD to the desorption isotherm would incorrectly skew the PSD to smaller pore widths.

Accuracy of the Adsorption Model. The crucial step in assembling accurate model isotherms from nonlocal theory is to obtain the best possible estimate of the solid–fluid potential parameters. To do so, it is desirable to fit to the isotherm of a nonporous sorbent that has a surface which closely resembles that of the porous specimens whose PSDs we wish to determine. The work presented here uses a nonporous isotherm measured on Vulcan carbon. Clearly it is unlikely that either the nonporous sample or the porous carbons of section 4.1 actually have ideal graphitic surfaces. While the pretreatment conditions should be sufficient to remove any physisorbed gases, the removal of chemisorbed species such as CO would require elevated temperatures that may alter the pore structure of the sorbent.[6] Hence, it is more accurate to view the solid–fluid parameters as representing the effective potential of a graphite-like surface. In this case, the main assumption in the model is that the surface concentration of functional groups is the same for pores of all widths. These factors may account for the differences in the nonlocal theory fit to the CXV isotherm at the monolayer filling pressure.

Another key assumption of the model is the neglect of connectivity in the modeling of adsorption in the individual pores. If the aspect ratio of pore length to pore width is in fact not large, then it is possible that the adsorption in a pore would be influenced by the condition of adjacent pores. This type of pore–pore correlation would complicate the solution of the adsorption integral.

Because the PSD results are obtained by assuming that all of the pores have a slit-shaped geometry, it is not possible to infer from the PSD additional information about the true morphology

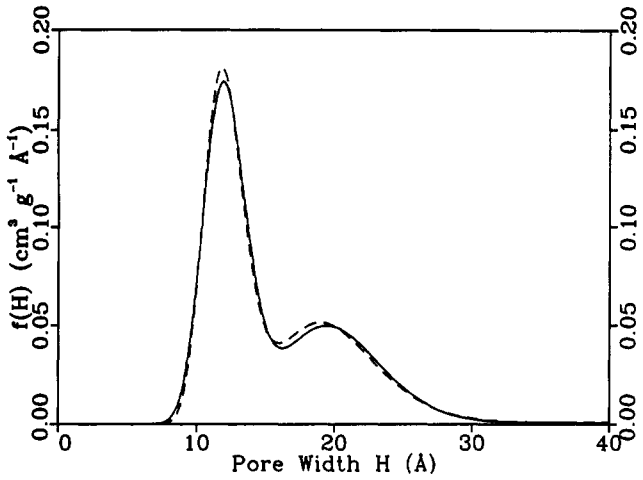

Figure 15. Test of numerical uniqueness of PSD of carbon AC610 obtained from nonlocal theory. The solid line shows the PSD fit calculated using the trimodal gamma distribution; the dashed line shows the PSD fit generated from the trimodal lognormal distribution. The two functional forms yield essentially identical results.

of the sorbent. In principle it is possible to add shape heterogeneity to the modeling of the pore structure, although this necessarily complicates solution of the adsorption integral, as discussed in section 2.1. There is experimental evidence[7] suggesting that the carbon pores have a slitlike geometry. Alternatively, the use of triangular-shaped pores of uniform size has been proposed[34] as a model for microporous carbon. This geometry introduces a energetic heterogeneity due to the pore shape, which gives better agreement to experimental measurements of the isosteric heat of adsorption than is obtained using uniformly sized slit pores as a model. However, Aukett et al.[19] demonstrated that it is possible to model the molar heat of adsorption of methane on carbon by using a size distribution of slit-shaped pores, a similar approach as is used in this work for modeling nitrogen adsorption. By use of a distribution of pore sizes, a different sort of heterogeneity is introduced which nonetheless seems equally capable of modeling calorimetric data for porous carbons.

Finally, we point out that there is no theoretical limitation to modeling the PSD using supercritical adsorption data, in place of the subcritical isotherms presented in this analysis. Indeed, it would be advantageous to compare, for consistency, the PSD results derived from measurements at multiple temperatures. However, the interpretation of the supercritical isotherms may prove more difficult, as the filling transitions in these isotherms tend to be less distinct than the condensation jumps observed in subcritical isotherms.

Mathematical Considerations. The solution of eq 5 presents a difficulty in that we are attempting to construct part of an integrand, $f(H)$, from information about the integral $N(P)$. In principle, this mathematical problem is ill-posed and will not give a unique solution for $f(H)$ unless an infinite number of data points $N(P)$ are available.[35] In practice, however, we have found that a sufficiently large sample of data (typically 30–50 points) constrains the shape of $f(H)$ such that the numerical values of the pore size distribution will essentially be the same, provided a sufficiently flexible functional form is chosen for the PSD. The functional form of $f(H)$ itself is arbitrary; any description that is suitably flexible to model the carbon PSD is acceptable, provided that the function is nonnegative over all pore widths. To verify the uniqueness of the numerical values of the PSDs, the fitting process was attempted using the trimodal lognormal distribution in place of the trimodal gamma distribution. As an example, we show in Figure 15 the predicted AC610 PSDs using the two functional forms; it is found that the lognormal distribution results are essentially indistinguishable from the gamma distribution results.

There are some fluctuations of the fitted isotherms about the experimental isotherms that might suggest a constraint imposed by the fitting procedure, given that the nonlocal theory model of adsorption seems accurate. Thus we are presently considering the adaptation of other convolution techniques to the solution of the adsorption integral.

For a review of the regularization methods for the solution of adsorption integrals, we refer the reader to ref 35.

5. Conclusion

The pore size distribution analysis method presented in this work offers a more quantitatively accurate approach to determining the PSD of carbons than previous methods have afforded. Because the method is based upon an improved molecular description of adsorption, the PSD results are more reliable than other analysis methods which do not correctly describe micropore filling. The nonlocal theory and fitting routine can accommodate other pore geometries, such as cylinders; thus, the analysis method is applicable to other porous materials, such as silicas, for example, which are conveniently modeled using a size distribution of cylindrical pores. In our continuing studies, we intend to apply the model to other adsorbate–adsorbent systems and other state conditions, and also to heat of adsorption data. We shall also develop additional tests of the robustness of the method, including comparison to other experimental results, and from self-consistency checks of the PSD analysis using different gases on the same adsorbent.

In view of the uncertainty regarding connectivity effects in the modeling of the PSD, it is timely to develop pore junction models to investigate these features. Hence, we are presently studying the adsorption and desorption of gases in simple porous networks using molecular simulation methods. Conceivably, it will prove possible to integrate connectivity effects into the PSD description of individual pores described in this work, thus providing a more complete theory of adsorption.

Our PSD model does not explicitly account for several other effects that are expected to be present in most porous materials: variations in pore shape and length, chemical heterogeneity, etc. It is hoped that the distribution of slit pores model used here may take these effects into account in some effective way. Careful tests, using molecular simulation and experiment, are needed to determine whether these neglected effects exhibit signatures in experimental results that are distinct from the PSD effects, and must therefore be explicitly taken into account.

Acknowledgment. We thank S. M. Riddiford, P. Aukett, and C. Jessop of BP Research for providing the experimental data for the carbons discussed in the text. C. Lastoskie is a National Science Foundation Fellow. N. Quirke thanks BP Research for permission to publish. We are grateful to the National Science Foundation for support of this work under Grants CTS-9122460 and INT-8913150.

References and Notes

(1) Sing, K. S. W.; Everett, D. H.; Haul, R. A. W.; Moscou, L.; Pierotti, R. A.; Rouquerol, J.; Siemieniewska, T. *Pure Appl. Chem.* **1985**, *57*, 603.
(2) Cranston, R. W.; Inkley, F. A. *Adv. Catal.* **1957**, *9*, 143.
(3) Brunauer, S.; Mikhail, R. S.; Bodor, E. E. *J. Colloid Interface Sci.* **1967**, *24*, 451.
(4) Walton, J. P. R. B.; Quirke, N. *Mol. Sim.* **1989**, *2*, 361.
(5) Evans, R.; Marini Bettolo Marconi, U. *Chem. Phys. Lett.* **1985**, *114*, 415.
(6) Bansal, R. C.; Donnet, J.; Stoeckli, F. *Active Carbon*; Marcel Dekker: New York, 1988; Chapters 2 and 3.
(7) Everett, D. H.; Powl, J. C. *J. Chem. Soc., Faraday Trans. 1* **1976**, *72*, 619.
(8) Horvath, G.; Kawazoe, K. *J. Chem. Eng. Jpn.* **1983**, *16*, 474.
(9) Saito, A.; Foley, H. C. *AIChE J.* **1991**, *37*, 429.
(10) Dollimore, D.; Heal, G. R. *J. Appl. Chem.* **1964**, *14*, 109.
(11) Kuwabara, H.; Takaomi, S.; Kaneko, K. *J. Chem. Soc., Faraday Trans.* **1991**, *87*, 1915.

(12) Gregg, S. J.; Sing, K. S. W. *Adsorption, Surface Area and Porosity*; Academic Press: New York, 1982.
(13) Davies, S.; Packer, K. J. *J. Appl. Phys.* **1990**, *67*, 3163. Davies, S.; Kalam, M. Z.; Packer, K. J.; Zelaya, F. O. *J. Appl. Phys.* **1990**, *67*, 3171.
(14) Davis, M. E.; Saldarriaga, C.; Montes, C.; Garces, J.; Crowder, C. *Zeolites* **1988**, *8*, 362.
(15) Johnson, J. W.; Brody, J. F. *Mater. Res. Soc. Symp. Proc.* **1988**, *111*, 257.
(16) Ramsay, J. D. F.; Booth, B. O. *J. Chem. Soc., Faraday Trans.* **1983**, *79*, 173.
(17) Ramsay, J. D. F.; Swanton, S. W.; Bunce, J. *J. Chem. Soc., Faraday Trans.* **1990**, *86*, 3919.
(18) Seaton, N. A.; Walton, J. R. P. B.; Quirke, N. *Carbon* **1989**, *27*, 853. Jessop, C. A.; Riddiford, S. M.; Seaton, N. A.; Walton, J. R. P. B.; Quirke, N. In *Characterization of Porous Solids II*; Rodriguez-Reinoso, F., Ed.; Elsevier Science: Amsterdam, 1991; pp 123–132.
(19) Aukett, P. N.; Quirke, N.; Riddiford, S.; Tennison, S. R. *Carbon* **1992**, *30*, 913.
(20) Lastoskie, C. M.; Gubbins, K. E.; Quirke, N. Submitted for publication in *Langmuir*.
(21) Steele, W. A. *Surf. Sci.* **1973**, *36*, 317; *The Interaction of Gases with Solid Surfaces*; Pergamon: Oxford, 1974.
(22) *CRC Handbook of Chemistry and Physics*, 61st ed.; Weast, R., Ed.; CRC Press: West Palm Beach, FL, 1981.
(23) de Boer, J. H.; Linsen, B. G.; Osinga, T. J. *J. Catal.* **1965**, *4*, 643.
(24) Evans, R. *Inhomogeneous Fluids*; Henderson, D., Ed.; Marcel Dekker: New York, 1992; Chapter 5.
(25) Tarazona, P. *Phys. Rev. A* **1985**, *31*, 2672; **1985**, *32*, 3148. Tarazona, P.; Marini Bettolo Marconi, U.; Evans, R. *Mol. Phys.* **1987**, *60*, 573.
(26) Carnahan, N. F.; Starling, K. E. *J. Chem. Phys.* **1969**, *51*, 635.
(27) Barker, J. A.; Henderson, D. *J. Chem. Phys.* **1967**, *47*, 4714.
(28) Telo da Gama, M. M. Unpublished data, 1985.
(29) Israelachvili, J. N. *Intermolecular and Surface Forces*, 2nd ed.; Academic Press: London, 1992.
(30) Balbuena, P. B.; Gubbins, K. E. *Fluid Phase Equilib.*, in press.
(31) Seaton, N. *Chem. Eng. Sci.* **1991**, *46*, 1895.
(32) Parlar, M.; Yortsos, Y. C. *J. Colloid Interface Sci.* **1989**, *132*, 425.
(33) Mason, G. *Proc. R. Soc. London, A* **1983**, *390*, 47.
(34) Bojan, M. J.; Steele, W. In *Proceedings of the Fourth International Conference on Fundamentals of Adsorption*, in press.
(35) v. Szombatheley, M.; Brauer, P.; Jaroniec, M. *J. Comput. Chem.* **1992**, *13*, 17.